Particle heating in localized Langmuir fields

W. Rozmus and P. P. Goldstein*
Department of Physics, University of Alberta, Edmonton, Alberta, Canada T6G 2J1
(Received 19 May 1988; revised manuscript received 21 July 1988)

Nonlinear particle dynamics are investigated in periodic, localized electrostatic fields which model a solution to the Zakharov equations. A large increase in the electron heating rates is observed and related to the partial destruction of the ponderomotive potential well. The threshold fields, for the increase in heating, are estimated from the overlap criterion and the analytical map which approximates motion of particles in the vicinity of the separatrix of the ponderomotive potential. Evolution of the distribution function and the averaged kinetic energy are also investigated.

I. INTRODUCTION

It is now evident that nonlinear theories of Langmuir waves can play an essential role in the interpretation of many plasma experiments. The modulational instability (in which the long-wavelength plasma wave breaks up into shorter wavelengths), the related formation of density cavities (by the ponderomotive force), self-focusing, and collapse of electrostatic field envelopes (leading to energy dissipation and production of hot particles) constitute the main elements of these theories called strong Langmuir turbulence (cf. Refs. 1, 2, and references therein).

In the original formulation[3] of the cavity dynamics, the cavity collapses practically without energy loss until the characteristic dimensions become comparable with the Debye radius. At this final stage of collapse the energy of electrostatic fields is transferred to electrons and the cavity burns out.

In this paper we propose a mechanism of energy dissipation and particle heating related to local, stochastic instability of electron trajectories in the nonlinear fields of Langmuir cavities. This model is relevant for one dimensional modeling and gives the threshold values of electrostatic field intensities beyond which the hydrodynamical formulations may become incorrect. The hydrodynamical model of strong Langmuir turbulence (the so-called Zakharov equations[3]) is based on the concept of the ponderomotive potential, which couples ion dynamics and high-frequency electrostatic fields. We will analyze the ponderomotive approximation from the point of view of particle dynamics, and show the conditions for which it loses its validity leading to rapid particle heating.

The physical context of our model is related to Langmuir waves produced, for example, during stimulated Raman-scattering (SRS) instabilities.[4,5] In the presence of stimulated Brillouin scattering (SBS) the SRS-produced Langmuir waves are modulated by the excited-ion density waves. The long-wavelength plasma modes break up into periodic localized structures separated by the distance defined by the ion-acoustic wavelength. A role similar to SBS-produced ion waves can be played by sound modes from the parametric decay instability. If there is no separate source of density modulations, the modulational instability of a broad envelope breaks it up into smaller sizes of a characteristic dimension inversely proportional to the initial field amplitude.

A number of authors have already studied, in theory[6,7] and experiments,[8] the nonlinear particle dynamics in the simple standing-wave configuration and found rapid increase in particle-heating rates once the threshold-field values are reached. In particular, Schmidt[7] discussed this effect in the context of the validity of the ponderomotive potential approximation.

In this paper we will first describe (Sec. II) the periodic localized structures given by the traveling-wave solutions to the Zakharov equations. The motion of the oscillation center will be studied in such fields in Sec. III. Analytic criteria for the resonance overlap (Sec. IV A), stochastic-layer formation in the vicinity of the separatrix (Sec. IV B), and conditions for total destruction of the ponderomotive potential (Sec. IV C) will be given. The numerical results of the evolution of the distribution function will be described in Sec. V. Conclusions and a summary are presented in Sec. VI.

II. LOCALIZED LANGMUIR FIELDS

Even for the simple case of one-dimensional, but driven Zakharov equations, analytical solutions are not known. Therefore, in proposing the form of electrostatic fields we have relied on the results of direct numerical integration[5] of the nonlinear equations and on the analytical solution to the much simpler, undriven nonlinear Schrödinger equation. The two main characteristics of numerical solutions, i.e., localization and periodicity, as well as the overall shape of the field envelope, are fairly well approximated by the combination of elliptic functions. The latter can be obtained from the Zakharov equations

$$i\frac{\partial}{\partial t}E+\frac{\partial^2}{\partial x^2}E=NE\ , \tag{1a}$$

$$\frac{\partial^2}{\partial t^2}N-\frac{\partial^2}{\partial x^2}N=\frac{\partial^2}{\partial x^2}|E|^2 \tag{1b}$$

if N can be assumed in the traveling-wave form $N(x-Vt)$. Equations (1) are written in a dimensionless form (cf., for example, Ref. 1) using the following units of time, distance, electric field E, and density fluctuations,

respectively,

$$\frac{3}{2}\frac{m_i}{m_e}\frac{1}{\omega_p},\ \frac{3}{2}\left[\frac{m_i}{m_e}\right]^{1/2}\lambda_D,\ 8\left[\frac{\pi n_e k_B T_e}{3}\frac{m_e}{m_i}\right]^{1/2},\ \frac{4}{3}n_e\frac{m_e}{m_i}. \tag{2}$$

By looking for solutions to Eqs. (1) in the form of a traveling wave $N=N(x-Vt)$, we effectively reduce the problem to the task of finding a solution to the nonlinear Schrödinger equation. Introducing the new variable

$$\xi=x-Vt, \tag{3}$$

we write the field envelope $E(\xi,t)$ in the following form:

$$E(\xi,t)=G_0(\xi)\exp[i\Phi(\xi,t)]. \tag{4}$$

Substituting expression (4) into Eqs. (1), separating them into relations for the amplitude G_0 and phase Φ, and integrating once, we obtain the following equation (cf. Appendix A),

$$\left[\frac{d}{d\xi}G_0\right]^2=C-\tfrac{1}{2}AG_0^2+\frac{1}{2W}G_0^4, \tag{5}$$

where three constants—C, A, and $W=V^2-1$—define the form of the solution.

For the purpose of studying nonlinear particle dynamics and to be in approximate agreement with numerical results,[5] we have chosen the subsonic case (in fact, we have assumed $V=0$, $W=-1$) and $A<0$, $C<0$. We can write solution for G_0 in the following convenient form,

$$G_0(x)=\frac{\alpha}{\sqrt{2}}[\mathrm{dn}(\alpha x,\beta+\beta\,\mathrm{cn}(\alpha x,\beta)], \tag{6}$$

where $x=\xi$; dn,cn are Jacobi elliptic functions[9] and the two parameters α and β are related to constants A and C in the following way:

$$A=-\alpha^2(1+\beta^2),\quad C=-\tfrac{1}{8}\alpha^4(1-\beta^2)^2. \tag{7}$$

The periodicity length of G_0, Eq. (6), as a function of variable x is given by $4K(\beta)/\alpha$, where K is the complete elliptic integral of the first kind.[9] Note two important limits of expression (6); first,

$$G_0(x)\underset{\beta\to 0}{\to}\frac{\alpha}{\sqrt{2}}(1+\beta\cos\alpha x) \tag{8}$$

and, second,

$$G_0(x)\underset{\beta\to 1}{\to}\frac{\alpha}{\sqrt{2}}(1+\beta)\frac{1}{\cosh\alpha x}. \tag{9}$$

Equation (8) describes small-amplitude modulations of the homogeneous field component [$K(\beta)\to\pi/2$] and the opposite limit of $\beta\to 1$ [$K(\beta)\to\infty$] corresponds to the solitonlike solution (9). The field amplitude can be measured in terms of the parameter

$$\frac{v_0}{v_e}=\frac{4}{\sqrt{3}}\left[\frac{m_e}{m_i}\right]^{1/2}E_{\max}, \tag{10}$$

where v_0 is the amplitude of the quiver velocity of an electron moving in the high-frequency field and v_e is the electron thermal velocity. The maximum value of the field amplitude is given by

$$E_{\max}=\frac{1}{\sqrt{2}}\alpha(1+\beta), \tag{11}$$

and it corresponds to $x=0,\pm 4K/\alpha,\ldots$.

Figure 1 gives an example of the field configuration (6). The particular choice of parameters corresponds to $v_0/v_e=0.97$; the periodicity length of the localized fields is relevant to Langmuir waves produced during SRS and modulated by SBS-produced ion waves at $n_e/n_{\mathrm{cr}}=0.2$ (where n_{cr} stands for the critical density) and $T_e=300$ eV. The characteristic wave number of ion waves is $k=0.097k_D$. We found in the numerical studies of the SRS-SBS evolution[5] that modulated long-wavelength Langmuir fields become more intense and very localized, but show no evident change in the periodicity length. This also seems to be a characteristic feature of the numerical solutions to the Zakharov equations, where the wavelength of the fastest-growing mode of the modulational instability determines periodicity of the localized structures at later times. By taking this into account in our model we are able to relate coefficients α and β. Let us assume that the wave vector k_p determines a characteristic periodicity length

$$\frac{2\pi}{k_p}=\frac{4K(\beta)}{\alpha}. \tag{12}$$

For the strongly localized fields ($\beta\to 1$) we can approximate the elliptic integral K by[9]

$$K(\beta)\simeq\ln\left[\frac{4}{(1-\beta^2)^{1/2}}\right]. \tag{13}$$

Substituting expression (13) in Eq. (12) and solving for β, we obtain

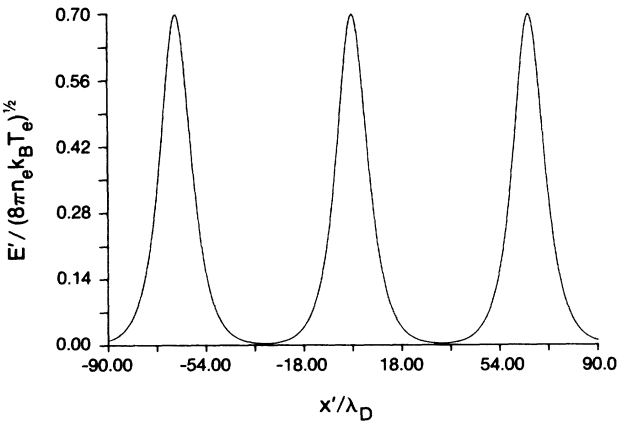

FIG. 1. Example of an electrostatic field given by Eq. (6). E' and x' stand for field and distance in dimensional units. Characteristic parameters are $\alpha=3$, $\beta=0.9875$ ($m_i/m_e=100$). They correspond to $v_0/v_e=0.97$ [Eq. (10)] and $k_p=0.097k_D$ [Eq. (12)].

$$\beta^2=1-16\exp\left[-\frac{\pi\alpha}{k_p}\right] . \tag{14}$$

Our analysis of particle dynamics, stability of the ponderomotive potential, and particle heating will be based on the solutions of the equations of motion in high-frequency electrostatic fields. The fields have the form

$$G(x,t)=G_0(x)\cos[(\Omega_p-\tfrac{1}{2}A)t]$$
$$\simeq E(x)\cos(\Omega_p t) , \tag{15}$$

where G_0 is defined by Eq. (6) and correction to the plasma frequency defined by constant A, Eq. (7), is usually much smaller than Ω_p (within the parameter range discussed below). Assuming that we can drop this extra term in frequency, our expression for G_0 [Eq. (6)] defines the field envelope E [cf. Eq. (1)].

III. MOTION OF THE OSCILLATION CENTER

The hydrodynamical model based on the Zakarov equations (1) relies on the validity of the ponderomotive potential approximation. For electrons moving in the electrostatic field (15), the equation of motion has the following form:

$$\frac{d^2}{dt^2}x(t)=-\frac{6}{\sqrt{3}}\frac{m_i}{m_e}E(x)\cos\Omega_p t , \tag{16}$$

where we have used the Zakharov units [Eq. (2)]. If the field amplitude is not too large, one can separate particle trajectory into oscillations of period $T_p=2\pi/\Omega_p$ about an oscillation center that moves on the slower time scale. Writing $x=x_f+x_s$ where s stands for slow and f for fast, one obtains, approximately, for the fast variable,

$$\frac{d^2}{dt^2}x_f=-\frac{6}{\sqrt{3}}\frac{m_i}{m_e}E(x_s)\cos\Omega_p t , \tag{17}$$

with the solution

$$x_f=\frac{6}{\sqrt{3}}\frac{m_i}{m_e}\frac{1}{\Omega_p^2}E(x_s)\cos\Omega_p t , \tag{18}$$

provided that $x_f\ll 1$ or $E_{\max}\ll m_i/m_e$ ($\Omega_p=1.5m_i/m_e$). Expanding

$$E(x_f+x_s)\simeq E(x_s)+x_f\frac{d}{dx_s}E(x_s)+\cdots , \tag{19}$$

we obtain an approximate equation for the slow variable from (18) and (19),

$$\frac{d^2}{dt^2}x_s=-3\left[\frac{m_i}{m_e}\right]^2\frac{1}{\Omega_p^2}\left[\frac{d}{dx_s}E^2(x_s)\right](1+\cos2\Omega_p t) , \tag{20}$$

where the last term in small parentheses vanishes after averaging over the fast time. Finally,

$$\frac{d^2}{dt^2}x_s=-\frac{d}{dx_s}\Phi_p(x_s) \tag{21}$$

is the equation of motion of the oscillating center, equivalent to the motion of a particle in the ponderomotive potential,

$$\Phi_p=3\left[\frac{m_i}{m_e}\right]^2\frac{1}{\Omega_p^2}E^2 . \tag{22}$$

Figure 2 shows the typical phase space of particles moving in the electrostatic field (15), plotted in Fig. 1. This surface of section mapping, obtained from numerical solution of the equation of motion (16), plots position and velocity at every plasma period. Figure 2 displays the region of regular trajectories near zero velocity. Particles in this region experience ponderomotive potential (15) and, if the initial distribution function is a Maxwellian, the bulk of the particles is trapped between the localized fields.

Adjacent to the area with ponderomotive force, we find irregular trajectories which almost uniformly fill the bounded part of the phase space. These particles form characteristic high-energy tails in the distribution function and are responsible for energy absorption. We have proposed a diffusion model[10] in order to describe time evolution of the particle distribution function in this velocity range. The results indicate moderate heating which should be included in Zakharov model.

We have observed here, however, the rapid increase in heating rates for large field amplitudes which correspond to destruction of regular orbits in the region described by the ponderomotive potential and to formation of the region of interconnected stochasticity. [The destruction of last Kolmogorov-Arnol'd-Moser (KAM) surface cuts into separate pieces the chain of resonances at zero phase velocity.] This, in turn results in a very large energy absorption by particles, because the process involves almost the whole bulk of the distribution function. For the hydrodynamical evolution of electrostatic fields (15), these

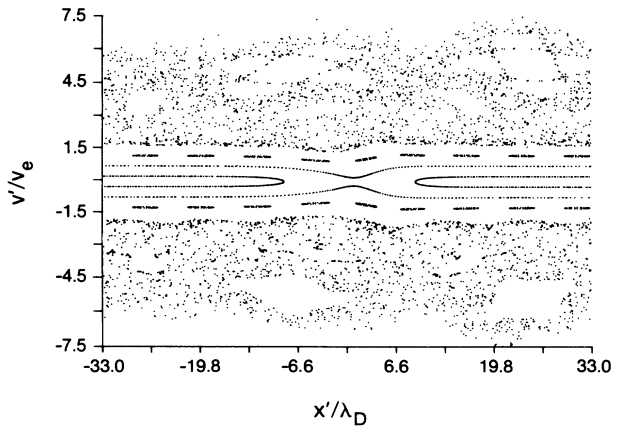

FIG. 2. The Poincaré surface of the section plot, based on numerical solutions to the equation of motion (16) with electrical field E as in Fig. 1. Points are mapped every $T_p=2\pi/\Omega_p$; v' and x' are dimensional velocity and position, respectively.

processes set up the limit of validity of the ponderomotive approximation and they play a role which is similar to wave-breaking phenomena in the case of a plane wave.

IV. VALIDITY OF THE PONDEROMOTIVE POTENTIAL APPROXIMATION

A. Resonance overlap

Our objective is to determine field intensities for which two regions of mixing (Fig. 2), at positive and negative velocities, will interconnect. Such a transition to global stochasticity can be determined using the overlap criterion.[11] The latter postulates that the last KAM surface between two resonances is destroyed if the distance between modes, measured, for example, in terms of difference between phase velocities, is equal to the sum of the half-widths of the two island separatrices formed by the resonances. In spite of the fact that this criterion can only give approximate values of the field, it usually predicts the extent of the stochastic regions with sufficient accuracy and it has been successfully applied in a similar problem[12] (cf. also Ref. 10). The resonance-overlap critierion can be made more accurate by taking into account the finite width of the stochastic layers in the vicinity of the separatrices (see next subsection).

The electrostatic field (15) can be represented in terms of a Fourier series.

$$G(x,t)=\frac{1}{\sqrt{2}}k_p\left[\cos\Omega_p t+2\times\sum_{\substack{m=-\infty\\ m\neq 0}}^{\infty}Q_{|m|}\cos(mk_p x-\Omega_p t)\right], \tag{23}$$

where $Q_m=q^{m/2}/(1+q^m)$, $q=\exp[-\pi K'(\beta)/K(\beta)]$, $K'(\beta)=K((1-\beta^2)^{1/2})$, and k_p is given by (12). The field (23) has a uniform component which approximately corresponds to a long-wavelength Langmuir wave, which in the process of nonlinear evolution is modulated and evolves into a chain of localized structures. In a sightly more general situation, this component of the wave packet can have its own finite k number and the field G would have the Bloch function form (cf. Ref. 10). We found that the presence of this extra plane wave, apart from changing the structure of the modes, does not affect the form of the ponderomotive potential well.[10] It introduces asymmetry into the phase-space plots, but it should not qualitatively change the transition to global stochasticity.

The equation of motion (16) can now be written in the following form:

$$\frac{d^2}{dt^2}X(t)=-\sum_{m=-\infty}^{\infty}A_m\cos(mk_p x-\Omega_p t)\ , \tag{24}$$

where

$$A_m=\sqrt{6}\frac{m_i}{m_e}k_p Q_{|m|}\ .$$

We have plotted the amplitudes A_m as functions of the phase velocity of the modes $v_{\rm ph}^{(m)}=\Omega_p/mk_p$ in Fig. 3. This plot corresponds to physical parameters of the map shown in Fig. 2. The horizontal lines in Fig. 3 give the width of the trapping regions,

$$2v_{\rm trap}^{(m)}=8\left[\frac{1}{mk_p}A_m\right]^{1/2}, \tag{25}$$

calculated separately for each mode.

The stochastic regions in Fig. 2 are defined by the overlapping modes $m=2,\ldots,6$ as shown in Fig. 3. Although modes 7 and 8 seem to overlap weakly in Fig. 3, their amplitudes are very small and the corresponding trapping regions are separated from the stochastic part of the phase space. This is more apparent in Fig. 4, which shows the magnified portion of Fig. 2 in the vicinity of the ponderomotive potential. It displays trajectories of particles predominantly interacting with modes: 7 ($v_{\rm ph}=\pm 1.47v_e$), 8 ($v_{\rm ph}=\pm 1.29v_e$); also, regular orbits trapped by waves 9 ($v_{\rm ph}=\pm 1.15v_e$) and 10 ($v_{\rm ph}=\pm 1.03v_e$) are clearly visible.

Finally, the shaded part of Fig. 3 represents the width of a ponderomotive potential. From (21) and (22) one can easily find the maximum velocity of the particle still trapped by the ponderomotive potential to be

$$v_s^{\max}=\frac{4}{\sqrt{3}}\alpha\sqrt{\beta}=\frac{\sqrt{2\beta}}{1+\beta}\left[\frac{m_i}{m_e}\right]^{1/2}\left[\frac{v_0}{v_e}\right]. \tag{26}$$

For the parameters of Figs. 1–4, $v_s^{\max}=0.69v_e$.

As the field amplitude increases, and k_p remains constant, the trapping width of the ponderomotive potential (26) grows and may finally link with the stochastic regions defined by the overlapping modes. At this point we should expect dramatic increase in particle heating as thermal electrons can now access high-velocity regions.

The overlap condition for the ponderomotive potential

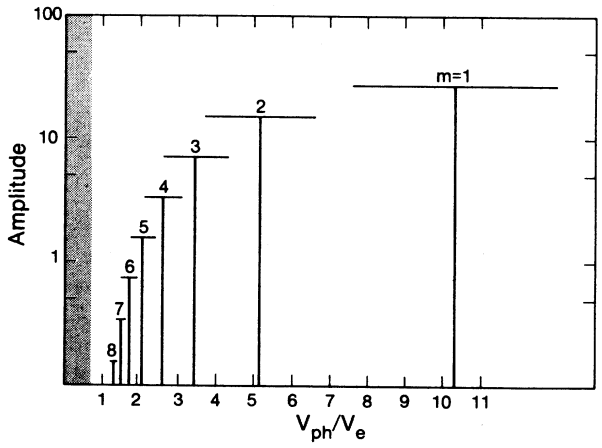

FIG. 3. The amplitudes A_m [Eq. (24)] of the Fourier modes in velocity space ($m_i/m_e=100$), for the parameters of Figs. 1 and 2. The full separatrix width of a mode is indicated by the horizontal line. The shaded region corresponds to the trapping width of the ponderomotive potential. Only the modes with positive phase velocities are plotted.

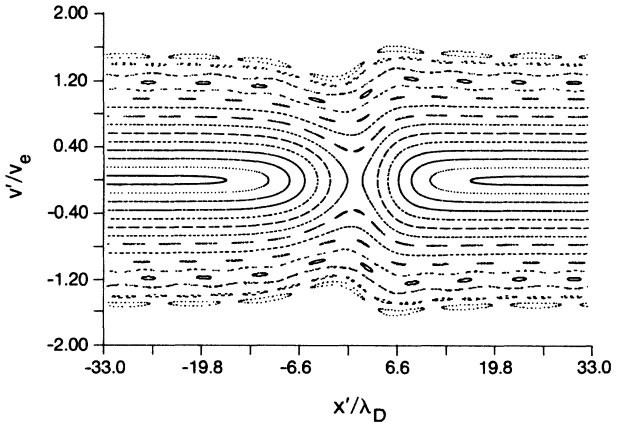

FIG. 4. The surface of the section plot generated for the same conditions as Fig. 2 with the region of small velocities enlarged.

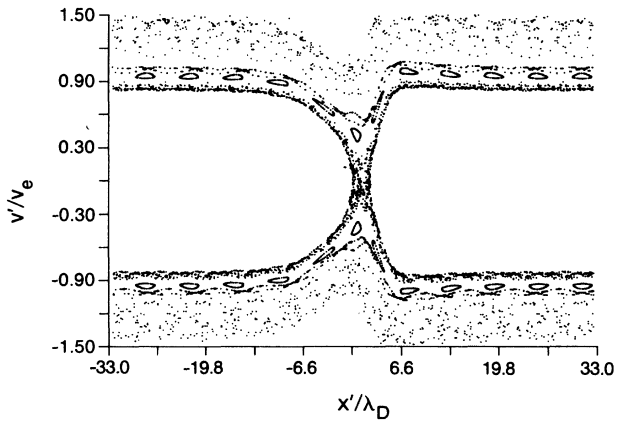

FIG. 5. The surface of the section plot for $v_0/v_e=1.22$ and k_p as in Fig. 1. The vicinity of the separatrix of the ponderomotive potential displays apparent asymmetry as $x'\rightarrow -x'$ and $v'\rightarrow v'$ (similar to Figs. 4 and 6), while the equations of motion (21) in the ponderomotive potential are symmetric with respect to this transformation. Note, however, that the map has been constructed from the numerical solutions of the full equations of motion (16) which do not have the symmetry $x\rightarrow -x$, $t\rightarrow -t$ (i.e., $x\rightarrow -x$, $v\rightarrow v$). Also, taking snapshots of exact trajectories every $T_p=2\pi/\Omega_p$ is not equivalent to the procedure leading to the ponderomotive approximation (21), particularly at higher field amplitudes.

and mode m from the stochastic part of the phase space can be expressed in the following form:

$$v_s^{\max}+v_{\text{trap}}^{(m)}>\frac{\Omega_p}{mk_p}\ . \tag{27}$$

In addition, the trapping of mode m must overlap with the $m-1$ component of the wave packet, i.e.,

$$v_{\text{trap}}^{(m)}+v_{\text{trap}}^{(m-1)}>\left|\frac{\Omega_p}{(m-1)k_p}-\frac{\Omega_p}{mk_p}\right|\ , \tag{28}$$

which at this point is already connected with mode $m-2$, and so on.

We shall illustrate the above theoretical discussions by giving a few numerical examples. Figures 2 and 4 display, apart from the regions of local stochasticity at higher velocities, well-ordered phase space with a majority of particles trapped on regular orbits between localized fields (maximum field intensity at $x=0$ corresponds to $v_0/v_e=0.97$, and k_p is $0.097k_D$ in dimensional units).

At $v_0/v_e=1.22$, and the same k_p, Eq. (12) (Fig. 5), the vicinity of separatrix of the ponderomotive potential exhibits regular orbits belonging to resonances 10 ($v_{\text{ph}}=1.03v_e$) and 11($v_{\text{ph}}=0.94v_e$), while modes 9 and 8 seem to overlap. Another important element of Fig. 5 is the stochastic layer formed at the separatrix of the ponderomotive potential. Formation of this layer contributes to the local destruction of the zero-order resonance and to the transition to global stochasticity by facilitating mode overlap.

Figure 6 shows what happens for $v_0/v_e=1.31$ [and the same k_p, Eq. (12), as in Figs. 4 and 5]. Most of the slow and thermal particles are still moving on regular orbits trapped between localized structures. The regions of stochastic motion have been extended almost up to separatrices of the ponderomotive potential. The stochastic strip around the separatrix is clearly visible, but still quite narrow and separated from regions of interconnected stochasticity at high velocities.

The mode-overlap criteria [Eqs. (27) and (28)] suggest that for this case mode 11 should weakly overlap with the ponderomotive potential and faster modes in the wave packet. Obviously, this field amplitude is not sufficient to break up chain of resonances in the vicinity of zero velocity. As we shall see below, this will happen around $v_0/v_e=1.6$ when the overlapping criteria (27) and (28) predict overlap between mode 8 and the ponderomotive potential. Also, our estimate of the stochastic layer will predict considerable width for the latter case.

The regions of interconnected stochasticity may be seen in Fig. 7 for $v_0/v_e=1.8$. It is clear that Fig. 7 represents a qualitatively different situation from Figs. 6 and 4. Now a large part of bulk electrons can be accelerated and access regions of high, positive and negative, velocities. It is also the case of the strong mode overlap as seen in Fig. 8. It is interesting to note, howev-

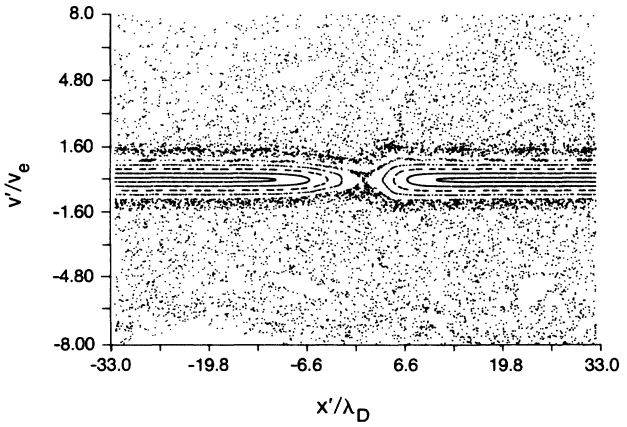

FIG. 6. The surface of the section plot for $v_0/v_e=1.31$ and the same k_p as in Figs. 2 and 3.

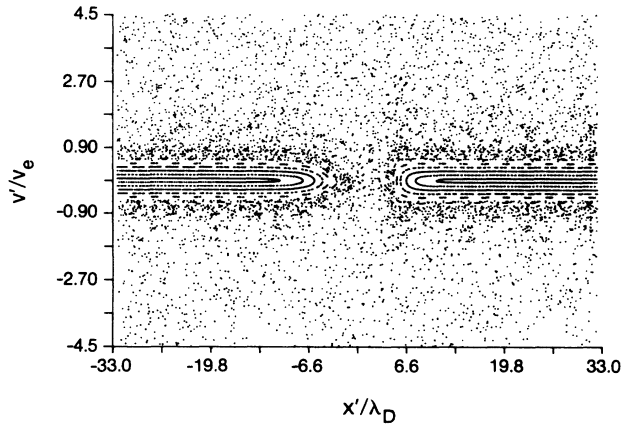

FIG. 7. The surface of the section plot for $v_0/v_e=1.8$ and k_p as in Figs. 2 and 3.

er, that even in the case of these fairly strong fields the trapping region of mode 1 is separated from the stochastic part of the phase space. In practical terms this will indicate strong energy absorption but lower-energy electrons produced by wave-particle interactions.

So far we have discussed the case of constant periodicity length $2\pi/k_p$ and different values of field intensities. One can think, however, about various physical conditions when Langmuir waves get modulated with different k_p. The interesting case occurs when k_p becomes smaller; then, $K(\beta)$ [cf. Eq. (12)] grows at given α, and β reaches values very close to unity for localized fields. The Fourier series (23) will have many components with physically interesting values of k, i.e., smaller than k_D. The overlapping criterion (27) will be more difficult to satisfy, mainly because $v_{\text{trap}}^{(l)}\sim 1/\sqrt{l}$ and one has to consider higher harmonics in order to reach the same value of mk_p and phase velocity as compared to larger k_p. Note that q in the definition of A_m (24) is now very close to unity. At the same time, harmonics with smaller k_p can

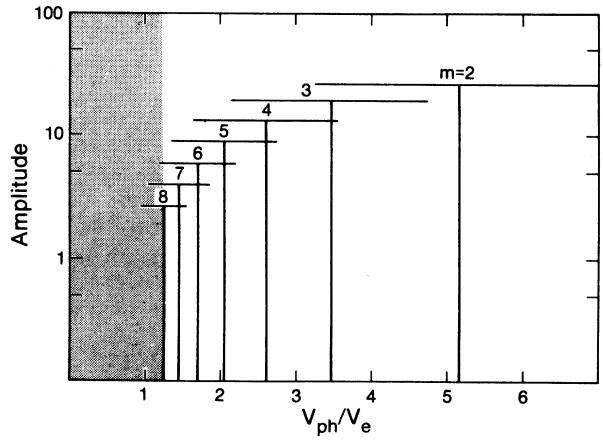

FIG. 8. The amplitudes A_m [Eq. (24)] in velocity space, for the parameters of Fig. 7. Mode $m=1$ is still separated from the overlapping waves ($m=2,\ldots,8$). The shaded region corresponds to the trapping width of the ponderomotive potential.

overlap much more easily between themselves and diffuse particles into the hot tails (cf. Ref. 12) more effectively.

B. Stochastic-layer formation

The calculations in this subsection describe formation of the stochastic layer in the vicinity of the separatrix of the ponderomotive potential. They paraphrase the standard approach to this problem described by Chirikov[11] for the case of a nonlinear pendulum. The results of this derivation are valid only close to the separatrix and therefore they describe local effects in the phase space. We have found, however, that a transition to global stochasticity corresponds to the same field intensities as formation of the stochastic layer of a considerable width. Therefore the estimates given below can supplement overlapping criteria; in particular, they can help to determine which mode from the wave packet should overlap with the ponderomotive potential well for the transition to global stochasticity to occur.

We first investigate the equation of motion (20) for the particles moving primarily under the influence of ponderomotive force. The oscillatory term in Eq. (20), which describes the coupling between high-frequency oscillations and the motion of the oscillation center, will be treated as a disturbance. The Hamiltonian function related to variables x_s can be written in the following form:

$$H=H_s+V(x_s,t) \tag{29}$$

and

$$\begin{aligned} H_s&=\tfrac{1}{2}(\dot{x}_s)^2+\Phi_p(x_s)\ , \\ V&=\Phi_p(x_s)\cos 2\Omega_p t\ . \end{aligned} \tag{30}$$

It is well known that even for arbitrarily small field amplitudes, the region around the separatrix of the nonlinear resonance exhibits stochastic particle motion.[11] The motion near the separatrix is extremely unstable since the separatrix divides regions of qualitatively different kinds of motion (oscillation and rotation), the transition between them being possible under very weak perturbation.

We shall first derive an approximate separatrix map[11] for the particle motion in the vicinity of the separatrix of the ponderomotive potential. Next, an estimate will be given for the width of the stochastic layer. Using this criterion, we will find the range of field amplitudes corresponding to a rapid increase in heating rates.

Let us start with analytical solution to the motion of the oscillation center $x_s(t)$. The energy H_s is a constant of motion C and can be written in the following form:

$$C=\tfrac{1}{2}(\dot{x}_s)^2+\tfrac{4}{3}E^2(x_s)\ , \tag{31}$$

where we used the explicit form of the plasma frequency $\Omega_p=1.5m_i/m_e$. For the motion on the separatrix the constant (31) is equal to

$$C_1=\tfrac{2}{3}\alpha^2(1+\beta)^2\ , \tag{32}$$

and the minimum value of the ponderomotive potential (maximum velocity), at $x_s=2K(\beta)/\alpha$, is given by

$$C_2=\tfrac{2}{3}\alpha^2(1-\beta)^2 . \tag{33}$$

In the vicinity of the separatrix we deal with two kinds of trajectories: for $C>C_1$ particles are untrapped and the motion corresponds to rotation, and for $C<C_1$ particles oscillate on closed orbits with characteristic frequency $\omega(C)$. Even in the first case ($C>C_1$) it still makes sense to introduce a characteristic frequency because our phase space is periodic. In order to calculate this frequency, we can first derive from Eq. (31) an expression of the oscillation center velocity,

$$\frac{dx_s}{dt}=[2(C-\phi_p)]^{1/2} . \tag{34}$$

Then, by using the simple relation

$$\frac{dx_s}{dt}=\frac{d\phi_p}{dt}\Big/\frac{d\phi_P}{dx_s}=\frac{d\phi_p}{dt}\Big/\left[\frac{4}{3}\frac{d}{dx_s}E^2\right] , \tag{35}$$

where we have used Eq. (22), we can write, for the time derivative of the ponderomotive potential,

$$\frac{d\phi_p}{dt}=\sqrt{3}[\phi_p(C-\phi_p)(C_1-\phi_p)(\phi_p-C_2)]^{1/2} . \tag{36}$$

In the equation above we have used expressions (5), (7), (22), (32), (33), and (34). By introducing a new variable $y=1/\phi_p$, we can rewrite Eq. (36) in the following form:

$$\frac{dy}{[(Cy-1)(C_1y-1)(1-C_2y)]^{1/2}}=-\sqrt{3}\,dt . \tag{37}$$

Equation (37) can be integrated along the trajectory between $x_s=0$ and $x_s=4K(\beta)/\alpha$, for $C>C_1$, and along half of the closed orbit for $C<C_1$, in order to obtain a period o the motion T,

$$T=\begin{cases}(4/\sqrt{3})[C_1(C-C_2)]^{-1/2}K(\kappa), & C>C_1\\ (4/\sqrt{3})[C(C_1-C_2)]^{-1/2}K(1/\kappa), & C<C_1\end{cases} \tag{38}$$

where K stands for the complete elliptic integral[9] and

$$\kappa^2=\frac{C}{C_1}\frac{C_1-C_2}{C-C_2} . \tag{39}$$

It follows from the properties of the elliptic integral that for the motion on the separatrix ($C\to C_1$) expression (39) diverges logarithmically to infinity. It takes infinite time for the particle to reach the points of maximum potential ($x_s=0,\ 4K/\alpha$). This is also one of the peculiarities of motion close to the separatrix, i.e., particles spend most of the time in the neighborhood of hyperbolic points $x_s=0,\ \pm K/\alpha,\ \ldots$, where velocity is almost zero. The rapid variation of velocity takes place over much shorter time and has an impulselike character.[11] We use this fact to introduce a discrete approximation to the motion close to the separatrix.

We need to calculate the change in the energy H [Eq. (29)] of the oscillation center during the time corresponding to the period T [Eq. (38)]. Instead of calculating the change in the full Hamiltonian (29), one may find that in unperturbed energy H_s we have

$$\frac{d}{dt}H_s=\{H,H_s\}=-\frac{\partial V}{\partial x_s}\frac{\partial H}{\partial \dot{x}_s} , \tag{40}$$

where $\{\ ,\ \}$ stands for the Poisson bracket. The last expression has a simple physical interpretation in terms of a disturbing force power, which, by using expression (30) for the potential V, can be written in the following form:

$$\frac{dH_s}{dt}=-\frac{\partial\phi_p}{\partial x_s}\frac{dx_s}{dt}\cos 2\Omega_p t . \tag{41}$$

The presence of $\dot{x}_s$ in Eq. (41) makes it possible to construct a pulse-to-pulse transformation. Note that between pulses, i.e., in the vicinity of hyperbolic points, $\dot{x}_s$ is very close to zero. We thus readily obtain, by integrating Eq. (41),

$$\Delta H_s=-\int_{\Delta t}d\tau\frac{dx_s}{d\tau}\frac{d\phi_p}{dx_s}\cos[2\Omega_p(\tau+\tau_0)] , \tag{42}$$

where the integral on the right-hand side is taken over a region Δt which includes the temporal width of the velocity pulse, and τ_0 is the initial time of the interaction. For motion close to the separatrix, one can set approximately $\dot{x}_s=v_{sx}$, $x_s=x_{sx}$, i.e., substitute the motion law at the separatrix for that one near the separatrix. We shall apply this simplification in Eq. (42) and extend the limits of integration to infinity. Expression (42) can now be written in the following form:

$$\Delta H_s=-\int_{-\infty}^{\infty}d\tau\frac{dx_{sx}}{d\tau}\left[\frac{d}{dx_{sx}}(\phi_p-C_1)\right]\cos[2\Omega_p(\tau+\tau_0)] , \tag{43}$$

where the constant C_1 was subtracted to simplify integration by parts, leading to

$$\Delta H_s=-2\Omega_p\int_{-\infty}^{\infty}d\tau[\phi_p(x_{sx}(\tau))-C_1]\sin[2\Omega_p(\tau+\tau_0)] . \tag{44}$$

Evaluation of the integral in Eq. (44) consists of two parts; first, we find the ponderomotive potential as a function of time, calculated on the separatrix $\Phi_p(x_{sx})$, and next we integrate it with the sine function by choosing the appropriate contour of integration. Details of these calculations are presented in the Appendix B and the final results (B11), reads

$$H_1-H_0=\Delta H_s=\frac{2\Omega_pC_1\pi\gamma}{\delta}\frac{1}{\sinh(\pi\Omega_p/\delta)}\times\sin\left[\frac{2\Omega_p}{\delta}\ln\left[\frac{1+\sqrt{\beta}}{1-\sqrt{\beta}}\right]\right]\sin\varphi_0 , \tag{45}$$

where

$$\gamma=[(C_1-C_2)/C_1]^{1/2},\quad \delta=\frac{\sqrt{3}}{2}C_1\gamma ,$$

where we have introduced the phase variable φ ($\varphi_0=2\Omega_p\tau_0$), which satisfies the equation

$$\frac{d\varphi}{dt}=2\Omega_p \ . \tag{46}$$

The discrete from of Eq. (46) defined the relation between phases of the distributing force before and after interaction,

$$\varphi_1-\varphi_0=2\Omega_p T(H_1) \ . \tag{47}$$

where the period T [Eq. (38)] corresponds to the motion with $C=H_1$. Equations (45) and (47) constitute the discrete approximation to the motion of the oscillating center in the vicinity of the separatrix. We will linearize Eq. (47) with respect to ΔH_s, Eq. (45), use an approximate form of the elliptic integral (13) in (38), and assume $C_2 \ll C_1$ $(\beta \to 1)$ to obtain

$$\varphi_1-\varphi_0=Q(H_0)+S(H_0)\sin\varphi_0 \ , \tag{48}$$

where

$$Q=\frac{8\Omega_p}{\sqrt{3}}\left[\frac{1}{C_1H_0}\right]^{1/2}\ln\left[4\left[\frac{C_1}{C_2}\frac{H_0}{|C_1-H_0|}\right]^{1/2}\right] , \tag{49}$$

$$S=\tfrac{16}{3}\pi\Omega_p^2\left[\frac{1}{C_1H_0}\right]^{1/2}\frac{1}{H_0}\left\{\ln\left[4\left[\frac{C_1}{C_2}\frac{H_0}{|C_1-H_0|}\right]^{1/2}\right]+\frac{C_1}{|C_1-H_0|}\right\}\frac{1}{\sinh(\pi\Omega_p/\delta)}\sin\left[\frac{2\Omega_p}{\delta}\ln\left[\frac{1+\sqrt{\beta}}{1-\sqrt{\beta}}\right]\right] . \tag{50}$$

The transition to chaos[11] takes place in the motion described by Eq. (48) when the parameter $|S|>1$. This relation for the given form of the field defines the width of the stochastic layer $|H_0-C_1|$ around the separatrix. Among the numerical examples given in the preceding subsection, Fig. 6 $(v_0/v=1.31)$ shows a narrow stochastic strip at the separatrix. The analytical model (45) and (48) predicts that in this case $|S|$ [Eq. (50)] reaches the values of order unity for the parameter $|H_0-C_1|/C_1\sim 0.0025$, which corresponds to the energy width of the stochastic layer of the order of 0.5% of C_1. Choosing the parameter $|H_0-C_1|/C_1$ of order 0.10, which gives the energy width of the stochastic layer of the order of 20% of C_1, we have $|S|\simeq 1$ if $v_0/v_e\simeq 1.63$. This is also the case when mode 8 (cf. Fig. 3) overlaps with the ponderomotive potential and a dramatic increase in heating rates (cf. Fig. 9) is observed. Finally, Fig. 7 shows the phase-space plot for $v_0/v_e=1.8$, where the parameter $|H_0-C_1|/C_1\simeq 0.1$ gives $|S|\sim 2.5$.

C. Total destruction of the potential well

To conclude this section , we look at another aspect of the transition to chaos. The results are less important for the transition to global stochasticity—they indicate the strong stability of the orbits at the bottom of the ponderomotive potential well.

Our computer-generated map shown in Fig. 2 gives rough indications about the existence of fixed points, periodic orbits which are just fixed points of the higher order. Half of these fixed points are stable, the other half are unstable. As the strength of the fields increases and localization becomes more pronounced, the stable fixed points destabilize, producing local chaos and more stable points close by. The destabilization of such orbits has been identified as the mechanism responsible for the spread of chaos (cf. Ref. 13, and references therein).

As an example we shall analyze the linear stability of the elliptic point corresponding to a minimum of the ponderomotive potential Φ_p [Eq. (22)] at $x_0=2K/\alpha$. This is the most stable point in the ponderomotive potential, and its destabilization corresponds to the total destruction of the potential well. Its stability properties can be deduced from the behavior of an adjacent point,

$$x(t)=x_0(t)+\xi \ , \tag{51}$$

where

$$x_0(t)=x_0+x_f(x_0) \ ,$$

and $x_f(x_0)$ is the oscillatory part, Eq. (18), of the solution, and $x_f \ll 1$. The equation of motion (16) with the field $E(x)$ defined by (6) is linearized around $x_0(t)$ [Eq. (51)], giving the following result:

$$\frac{d^2}{dt^2}\xi=-\frac{6}{\sqrt{3}}\frac{m_i}{m_e}\left[\frac{d^2E}{dx^2}\right]_{x=x_0}x_f(x_0)\cos^2\Omega_p t\,\xi \ , \tag{52}$$

where the second derivative of the electrostatic field (6) reads

$$\frac{d^2}{dx^2}E(x)=-\alpha^2\beta E(x)[\mathrm{cn}(\alpha x,\beta)\mathrm{dn}(\alpha x,\beta)-\beta\,\mathrm{sn}(\alpha x,\beta)]_{x=x_0=2K/\alpha}=\frac{\alpha^2\beta}{2}(1-\beta) \ . \tag{53}$$

Note that the first-order derivative of E, Eq. (6), evaluated at the stable point $x_0=2K/\alpha$ vanishes. Equation (52) can be rewritten in the following form:

$$\frac{d^2}{d\tau^2}\xi(\tau)+B_1(1+\cos\tau)\xi=0\ , \tag{54}$$

where the time variable is $\tau=2\Omega_p t$, and the constant is given by

$$B_1=\frac{4}{27}\left[\frac{m_e}{m_i}\right]^2\alpha^4\beta(1-\beta)^2$$
$$=\frac{1}{48}\left[\frac{v_0}{v_e}\right]^4\frac{\beta(1-\beta)^2}{(1+\beta)^4}\ .$$

Equation (54) is the Mathieu equation with stable solutions for small enough B_1. However, it destabilizes[14] at $B_1=0.19$. One therefore expects the complete breakdown of the ponderomotive potential at

$$\frac{v_0}{v_e}>1.76\frac{1+\beta}{\beta(1-\beta)^{1/2}}\ . \tag{55}$$

For the model analyzed in our paper, if the periodicity length is kept constant as the field strength increases [$4K(\beta)/\alpha=$const], the parameter β can reach values very close to unity and the inequality (55) is impossible to satisfy. For example, fields shown in Fig. 1 correspond to $\beta=0.9875$, which gives the threshold value of $v_0/v_e=31.5$. Thus, criterion (55) shows how stable the orbits are in the vicinity of the minimum of the ponderomotive potential. Equation (55) can have practical importance at small values of the field intensities, when v_0/v_e is not too large. In such cases we would, for example, exclude short-wavelength ion waves modulating Langmuir fields. It should be also emphasized that for fields much smaller than the threshold values (55), the destruction of regular orbits in the vicinity of the separatrix leads to the rapid spread of chaos and to particle heating which changes the hydrodynamical evolution of the fields.

V. EVOLUTION OF THE DISTRIBUTION FUNCTION

One of our major objectives in studying the destruction of the ponderomotive potential well and the transition to global stochasticity is the expected dramatic increase of hot-electron production. We shall illustrate this point by numerical calculations of the particle-heating rates and by giving the examples of the distribution functions. Our model assumes constant electric field amplitudes, and therefore it does not include any self-consistent effects; nevertheless, it can give useful indication of the strength of field necessary for large hot-electron production.

Figure 9 summarizes the dependence of the heating rates on the field amplitudes, while the characteristic periodicity of the localized fields is kept constant and corresponds to k_p (as in Fig. 1). The plot shows the ratio of an averaged kinetic energy per particle after 20 plasma periods to its initial value. The initial distribution function is a Maxwellian with parameters given below Eq. (11). On the time scale of 20 plasma periods, the time variation of the averaged kinetic energy is approximately linear; therefore Fig. 9 represents the heating rates as a function of field intensities. The increase in the heating rates is apparent for intensities corresponding to the partial destruction of the ponderomotive potential well seen in Fig. 7.

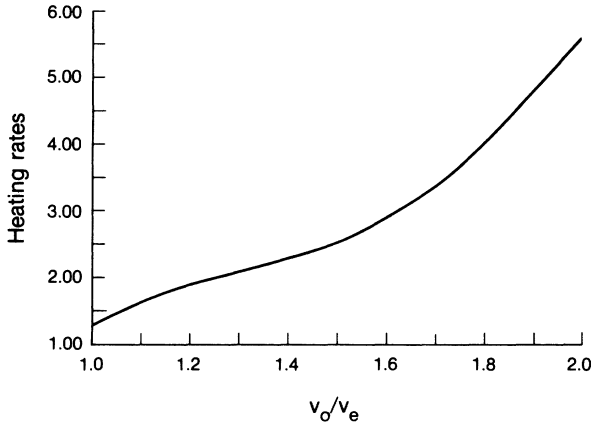

FIG. 9. Dependence of the heating rates on the field amplitudes. Vertical axis gives the ratio of the averaged kinetic energy per particle after 20 plasma periods to the initial one. Particles are evolved in the field configurations characterized by constant k_p (as in Fig. 1) and an initial Maxwellian distribution function. Horizontal axis gives v_0/v_e.

Figures 10 and 11 illustrate the increased electron heating by showing two examples of the distribution functions after 20 plasma periods. The comparison between the results at $v_0/v_e=1.0$ and 2.0 indicates two important reasons for the rapid transfer of wave energy into particles. First, in Fig. 10 one sees more particles from the bulk of the distribution function being accelerated into the tails at higher field intensity, which is the main consequence of the destruction of the ponderomotive potential well. Second, in Fig. 11 we see fully developed tails which also extend to much higher energies when $v_0/v_e=2.0$. The regions of mixing and stochastic insta-

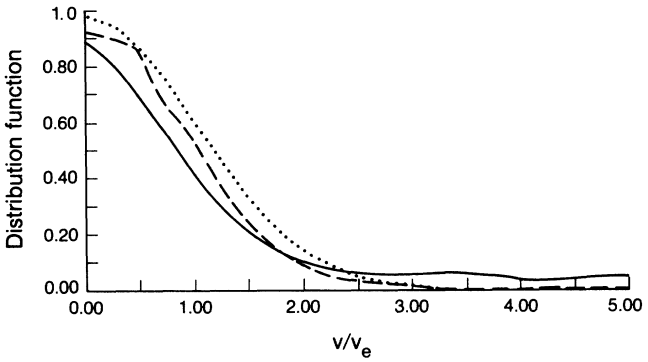

FIG. 10. Three particle distribution functions: dots, initial Maxwellian; long dash, field intensity during evolution corresponds to $v_0/v_e=1$; solid curve, $v_0/v_e=2$. The last two distributions are calculated after 20 plasma periods. Horizontal axis gives velocity in units of thermal velocity.

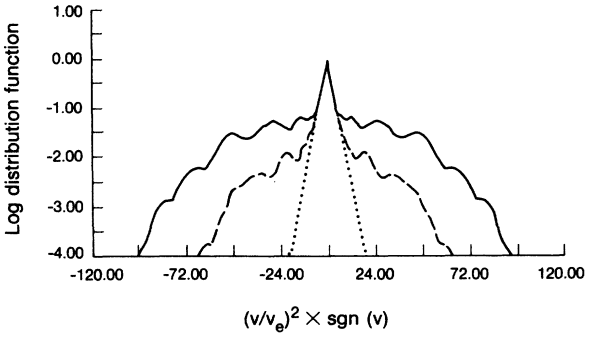

FIG. 11. Same as Fig. 7, but the vertical axis gives logarithms of the distribution functions plotted with respect to the kinetic energy of particles normalized to the thermal energy.

bility not only connect parts of the phase space with negative and positive velocities, but also extend themselves to much higher kinetic energies.

VI. CONCLUSIONS

We have analyzed particle dynamics in Langmuir fields which model the physical processes described by the Zakharov equations. In particular, we have investigated one of the possible mechanisms, which is related to stochastic instability of particles moving under the influence of the ponderomotive force, limiting the validity of a hydrodynamical description by the Zakharov equations.

The electrostatic fields are given by the combination of elliptic functions, for which we have kept the same periodicity length while changing the field amplitudes. Therefore we could reproduce in an approximate way the field evolution obtained in numerical analysis of the SBS/SRS problem,[5] or in the development of a modulational instability.

We have determined the threshold field intensity for the rapid increase in the electron-heating rate. This increase in heating is related to partial destruction of the ponderomotive potential well and the stochastic heating of particles from the bulk of the distribution function. Similar observations of rapid hot-particle production have been reported in the particle simulations[15] of the modulated Langmuir waves.

We have also found stable behavior of the particle orbits at the bottom of the ponderomotive potential well. The total destruction of the well requires very high field intensities. Depending on the strength of the source, the field evolution may be then altered by the formation of the large region of interconnected stochasticity and particle heating, or we can observe strongly localized fields leading to harmonic generation and strong Landau damping, as is usually assumed in the models of strong Langmuir turbulence. Finally, it is interesting to note that periodic localized electric field structures correlated with density depletions were recently found in the auroral acceleration region.[16] The mechanism of particle heating, described above, may also contribute to hot-electron production in magnetospheric plasmas.

ACKNOWLEDGMENTS

We would like to thank D. DuBois, H. Rose, and J. C. Samson for useful conversations and comments. One of us (P.P.G.) would like to acknowledge the very kind hospitality and support of Professor G. Rostoker during his stay at the University of Alberta. This research was supported in part by a Natural Sciences and Engineering Research Council (NSERC) of Canada operating grant held by W. Rozmus, and in part by a NSERC operating grant held by G. Rostoker.

APPENDIX A: DERIVATION OF EQ. (5)

Assume that N depends on x,t through a variable $\xi=x-VT$; only then,

$$N=|E|^2/W\ , \tag{A1}$$

where $W=V^2-1$ is the physically relevant solution of (1b). Inserting it into Eq. (1a) and substituting (4) for E, we obtain the following system of equations corresponding to the real and imaginary parts of (1a):

$$-G_0\left[\frac{\partial\phi}{\partial t}\right]_{\xi=\text{const}}+G_0\left[V\frac{\partial\phi}{\partial\xi}-\left[\frac{\partial\phi}{\partial\xi}\right]^2\right]+\frac{\partial^2 G_0}{\partial\xi^2}-\frac{G_0^3}{W}=0\ , \tag{A2}$$

$$\frac{\partial}{\partial\xi}\left[G_0^2\left[-\frac{V}{2}+\frac{\partial\phi}{\partial\xi}\right]\right]=0\ , \tag{A3}$$

where we have used $(\partial G_0/\partial t)_{\xi=\text{const}}=0$.

Equation (A3) may be integrated immediately (we limit our attention to the case in which the constant of integration is 0). Hence,

$$\phi=\frac{V}{2}\xi+\phi_0(t)\ , \tag{A4}$$

and, from (A4) and (A2),

$$\left[\frac{d\phi_0}{dt}\right]_{\xi=\text{const}}=\frac{V^2}{G_0}+\frac{1}{G_0}\frac{\partial^2 G_0}{\partial\xi^2}-\frac{G_0^2}{W}\ . \tag{A5}$$

The right-hand side does not depend on t when ξ is constant; therefore the left-hand side is also a constant, which, for the of convenience, will be set as $V^2/4+A/2$, $A=\text{const}$. Hence, we get

$$\frac{\partial^2}{\partial\xi^2}G_0=\frac{A}{2}G_0+\frac{G_0^3}{W}\ , \tag{A6}$$

from which (5) follows immediately.

APPENDIX B: CHANGE IN THE ENERGY OF THE OSCILLATION CENTER

Consider an integral in the expression (44) for the change in energy of the oscillation center

$$\Delta H_s=-2\Omega_p\int_{-\infty}^{\infty}d\tau[\phi_p(x_{sx}(\tau))-C_1]\times\sin[2\Omega_p(\tau+\tau_0)]\ . \tag{B1}$$

Following the steps outlined in calculations of the period T, Eq. (32), we first evaluate $\phi_p(x_{sx})$. Equation (36), for the motion on the separatrix $C=C_1$, takes the following form:

$$\frac{d\phi_p}{dt}=\sqrt{3}(C_1-\phi_p)[\phi_p(C-\phi_p)]^{1/2} . \tag{B2}$$

By introducing a new variable,

$$x=\left[1-\frac{C_2}{\phi_p}\right]^{1/2} , \tag{B3}$$

we can reduce Eq. (B2) to the following simple form:

$$\frac{dx}{\gamma^2-x^2}=\frac{\sqrt{3}}{2}C_1 dt . \tag{B4}$$

Integrating (B4), we obtain

$$\ln\left[\frac{\gamma+x}{\gamma-x}\right]=\sqrt{3}C_1\gamma(t-t_0) , \tag{B5}$$

where $\gamma=[(c_1-C_2)/C_1]^{1/2}$, and t_0 corresponds to the constant of integration. From (B5), after simple manipulations, we get the expression for the ponderomotive potential evaluated along the separatrix,

$$\phi_p(x_{sx}(t))=\frac{C_2}{1-\gamma^2\tanh^2[(\sqrt{3}/2)C_1\gamma(t-t_0)]} . \tag{B6}$$

Substituting Eq. (B6) into (B1), we have

$$\Delta H_s=2\Omega_p\int_{-\infty}^{\infty}d\tau\frac{C_1-C_2-C_1\gamma^2\tanh^2(\delta\tau)}{1-\gamma^2\tanh^2(\delta\tau)} \times\sin[2\Omega_p(\tau+\tau_0)] , \tag{B7}$$

where $\delta=(\sqrt{3}/2)C_1\gamma$. The essential part of the integral in Eq. (B7) can be written as

$$I_1=\int_{-\infty}^{\infty}d\tau e^{i2\Omega_p\tau} \times\frac{C_1-C_2-C_1\gamma^2\tanh^2(\delta\tau)}{\gamma^2[(1/\gamma)+\tanh(\delta\tau)][(1/\gamma)-\tanh(\delta\tau)]} . \tag{B8}$$

The integral above is related in a simple way to the integral over a closed contour running from $-\infty$ to $+\infty$ along the real axis and back from $+\infty$ to $-\infty$ along the line parallel to the real axis and separated from it by the distance $i\pi/\delta$ corresponding to the periodicity of the hyperbolic tangent. Only two simple poles at

$$\xi_{1\,(2)}=(+)(-)\frac{1}{2\delta}\ln\left|\frac{\gamma+1}{\gamma-1}\right|+i\frac{\pi}{2\delta} \tag{B9}$$

are encircled by this contour. Finding residua of Eq. (B8), we can write

$$I_1=\frac{\pi\gamma C_2}{\delta(1-\gamma^2)}\frac{1}{\sinh(\pi\Omega_p/\delta)} \times\sin\left[\frac{2\Omega_p}{\delta}\ln\left|\frac{\gamma+1}{\gamma-1}\right|\right] \tag{B10}$$

and, for the energy increase,

$$\Delta H_s=\frac{2\pi\Omega_p C_1\gamma}{\delta}\frac{1}{\sinh(\pi\Omega_p/\delta)} \times\sin\left[\frac{2\Omega_p}{\delta}\ln\left[\frac{1+\sqrt{\beta}}{1-\sqrt{\beta}}\right]\right]\sin(2\Omega_p\tau_0) . \tag{B11}$$

This is the increase of energy of the oscillation center during the motion close to separatrix due to the coupling between the slow and fast components of the motion.

*Visitor from the Institute for Nuclear Studies, Warsaw, Poland.

[1]M. V. Goldman, Rev. Mod. Phys. **56**, 709 (1984).

[2]A. M. Rubenchik, R. Z. Sagdeev, and V. E. Zakharov, Comments Plasma Phys. Controlled Fusion **9**, 183 (1985).

[3]V. E. Zakharov, Zh. Eksp. Teor. Fiz. **62**, 1745 (1972).

[4]C. M. Aldrich, B. Bezzerides, D. F. DuBois, and Harvey A. Rose, Comments Plasma Phys. Controlled Fusion **10**, 1 (1986); Harvey A. Rose, D. F. DuBois, and B. Bezzerides, Phys. Rev. Lett. **58**, 2547 (1987).

[5]W. Rozmus, R. P. Sharma, J. C. Samson, and W. Tighe, Phys. Fluids **30**, 2181 (1987).

[6]J. Y. Hsu, K. Matsuda, M. S. Chu, and T. H. Jensen, Phys. Rev. Lett. **43**, 203 (1979).

[7]G. Schmidt, Comments Plasma Phys. Controlled Fusion **7**, 87 (1982).

[8]F. Doveil, Phys. Rev. Lett. **39**, 532 (1981).

[9]E. Jahnke and F. Emde, *Tables of Functions* (Dover, New York, 1945).

[10]W. Rozmus, J. C. Samson, and A. A. Offenberger, Phys. Lett. **126A**, 263 (1988); W. Rozmus and J. C. Samson, Phys. Fluids (to be published).

[11]B. V. Chirikov, Phys. Rep. **520**, 263 (1979).

[12]V. Fuchs, V. Krapchev, A. Ram, and A. Bers, Physica **14D**, 141 (1985).

[13]A. J. Lichtenberg and M. A. Lieberman, *Regular and Stochastic Motion* (Springer-Verlag, New York, 1983).

[14]C. M. Bender and S. A. Orszag, *Advanced Mathematical Methods for Scientists and Engineers* (McGraw-Hill, New York, 1978).

[15]B. Bezzerides, C. H. Aldrich, D. F. DuBois, and H. A. Rose, Bull. Am. Phys. Soc. **32**, 1716 (1987).

[16]R. Boström, G. Gustafsson, B. Holback, G. Holmgren, H. Koskinen, and P. Kintner, Phys. Rev. Lett. **61**, 82 (1988).

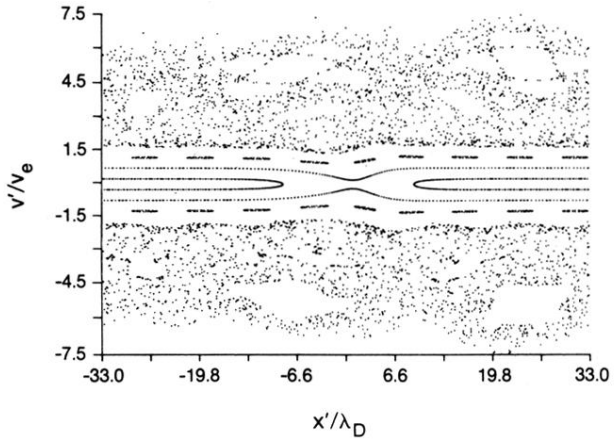

FIG. 2. The Poincaré surface of the section plot, based on numerical solutions to the equation of motion (16) with electrical field E as in Fig. 1. Points are mapped every $T_p = 2\pi/\Omega_p$; v' and x' are dimensional velocity and position, respectively.

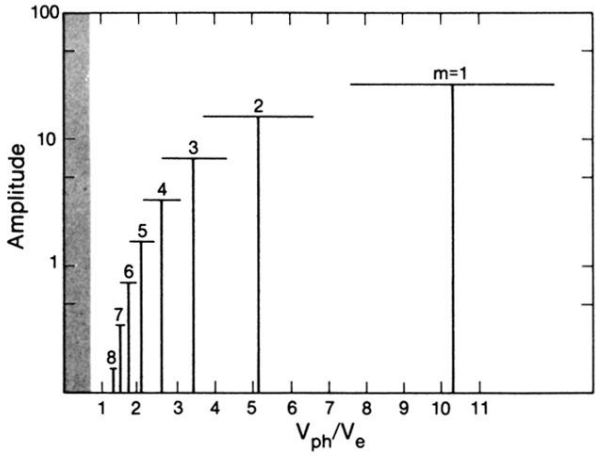

FIG. 3. The amplitudes A_m [Eq. (24)] of the Fourier modes in velocity space ($m_i/m_e = 100$), for the parameters of Figs. 1 and 2. The full separatrix width of a mode is indicated by the horizontal line. The shaded region corresponds to the trapping width of the ponderomotive potential. Only the modes with positive phase velocities are plotted.

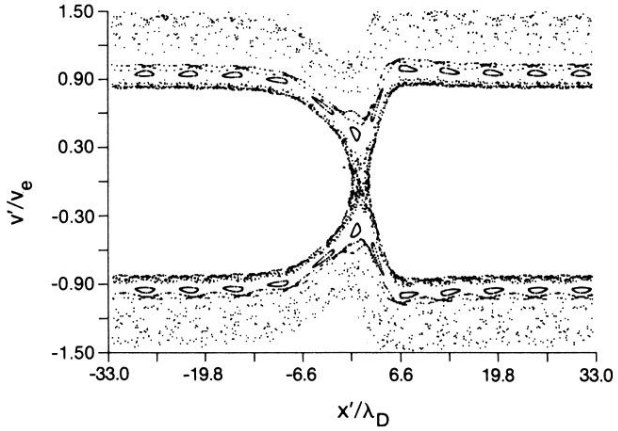

FIG. 5. The surface of the section plot for $v_0/v_e=1.22$ and k_p as in Fig. 1. The vicinity of the separatrix of the ponderomotive potential displays apparent asymmetry as $x'\rightarrow -x'$ and $v'\rightarrow v'$ (similar to Figs. 4 and 6), while the equations of motion (21) in the ponderomotive potential are symmetric with respect to this transformation. Note, however, that the map has been constructed from the numerical solutions of the full equations of motion (16) which do not have the symmetry $x\rightarrow -x$, $t\rightarrow -t$ (i.e., $x\rightarrow -x$, $v\rightarrow v$). Also, taking snapshots of exact trajectories every $T_p=2\pi/\Omega_p$ is not equivalent to the procedure leading to the ponderomotive approximation (21), particularly at higher field amplitudes.

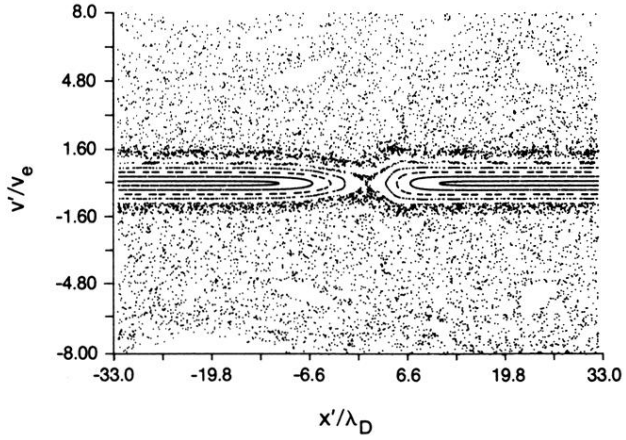

FIG. 6. The surface of the section plot for $v_0/v_e = 1.31$ and the same k_p as in Figs. 2 and 3.

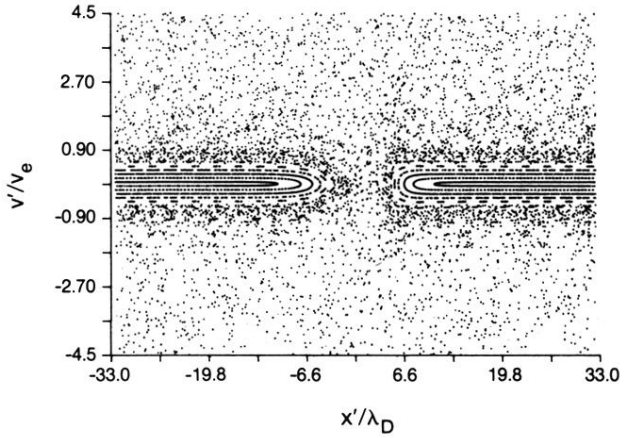

FIG. 7. The surface of the section plot for $v_0/v_e = 1.8$ and k_p as in Figs. 2 and 3.

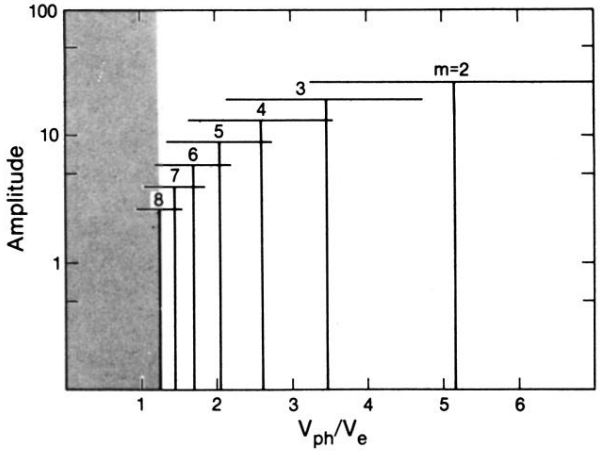

FIG. 8. The amplitudes A_m [Eq. (24)] in velocity space, for the parameters of Fig. 7. Mode $m=1$ is still separated from the overlapping waves ($m=2,\ldots,8$). The shaded region corresponds to the trapping width of the ponderomotive potential.